Structural Basis for Regulated Proteolysis by the α-Secretase ADAM10

Tom C.M. Seegar, Lauren B Killingsworth, Nayanendu Saha, Peter A Meyer, Dhabaleswar Patra, Brandon Zimmerman, Peter W Janes, Eric Rubinstein, Dimitar B Nikolov, Georgios Skiniotis, et al.

Structural Basis for Regulated Proteolysis by the α-Secretase ADAM10

Tom C.M. Seegar[1], Lauren B. Killingsworth[1], Nayanendu Saha[2], Peter A. Meyer[3], Dhabaleswar Patra[4], Brandon Zimmerman[1], Peter W. Janes[5], Eric Rubinstein[6], Dimitar B. Nikolov[2], Georgios Skiniotis[7], Andrew C. Kruse[1], Stephen C. Blacklow[1,8*]

[1]Department of Biological Chemistry and Molecular Pharmacology, Harvard Medical School, Boston, MA 02115, USA

[2]Structural Biology Program, Memorial Sloan-Kettering Cancer Center, New York, NY 10065, USA

[3]SBGrid Initiative, Harvard Medical School, Boston, MA 02115, USA

[4]Life Sciences Institute and Department of Biological Chemistry, University of Michigan, Ann Arbor, MI 48109, USA

[5]Department of Biochemistry and Molecular Biology, Monash University, Victoria 3800, Austraila

[6]Inserm and Université Paris-Sud, Institut André Lwoff, Villejuif, France

[7]Department of Molecular and Cellular Physiology, and Department of Structural Biology, Stanford University School of Medicine, Stanford, CA 94305 USA

[8]Lead Contact

[*]Correspondence to: stephen_blacklow@hms.harvard.edu

SUMMARY

Cleavage of membrane-anchored proteins by ADAM (a disintegrin and metalloproteinase) endopeptidases plays a key role in a wide variety of biological signal transduction and protein turnover processes. Among ADAM family members, ADAM10 stands out as particularly important because it is both responsible for regulated proteolysis of Notch receptors and catalyzes the non-amyloidogenic α-secretase cleavage of the Alzheimer's precursor protein, APP. We present here the X-ray crystal structure of the ADAM10 ectodomain, which together with biochemical and cellular studies reveals how access to the enzyme active site is regulated. The enzyme adopts an unanticipated architecture, in which the C-terminal cysteine-rich domain partially occludes the enzyme active site, preventing unfettered substrate access. Binding of a modulatory antibody to the cysteine-rich domain liberates the catalytic domain from autoinhibition, enhancing enzymatic activity toward a peptide substrate. Together, these studies reveal a mechanism for regulation of ADAM activity and offer a roadmap for its modulation.

INTRODUCTION

Proteolytic release of membrane-tethered proteins enables cells to interpret, communicate with, and respond to their microenvironment. ADAM (a disintegrin and metalloproteinase) endopeptidases are an abundant and diverse family of type-I transmembrane metalloproteinases that hydrolyze adhesion molecules, signaling receptors and growth factors. The human genome encodes 22 different ADAMs, essential for numerous developmental events (Weber and Saftig, 2012) including spermatogenesis, fertilization (Cho et al., 1998), immune and gastrointestinal system development (Jones et al., 2016), angiogenesis (Glomski et al., 2011), and development of the central nervous system (Jorissen et al., 2010; Kuhn et al., 2016). Moreover, dysregulated ADAM activity is implicated in a variety of pathophysiologic states, including asthma (Weskamp et al., 2006), infertility (Cho et al., 1998), Alzheimer's disease (Suh et al., 2013), and cancer (Murphy, 2008).

Among ADAM family members, ADAM10 stands out as having a particularly central role in both developmental signaling and disease pathogenesis. Physiologic Notch signaling, which is transduced by regulated intramembrane proteolysis (RIP), normally relies on ADAM10 proteolysis at a juxtamembrane site (called S2), followed by γ-secretase cleavage at the inner membrane leaflet at site S3 to release its intracellular domain as a transcriptional effector (Aster et al., 2017; Bray, 2016; Kovall et al., 2017). Other important ADAM10 substrates

identified from tissue specific knockouts, cell-based studies, and proteomic analyses include N-cadherin, pro-epidermal growth factor, betacellulin, HER2, NrCAM and ephrin receptors (Hartmann et al., 2002; Janes et al., 2005; Kuhn et al., 2016; Overall and Blobel, 2007; Reiss et al., 2005; Sahin et al., 2004).

In disease pathogenesis, ADAM10 has been implicated in the emergence of Herceptin resistance in breast cancer (Feldinger et al., 2014; Liu et al., 2006). It also has a prominent role in the non-amyloidogenic proteolytic shedding of the amyloid precursor protein (APP) as the major α-secretase in the central nervous system (Jorissen et al., 2010; Kuhn et al., 2010; Lammich et al., 1999), and deletion of ADAM10 in mouse neural progenitor cells results in markedly reduced APP processing at the neuroprotective α-secretase site (Jorissen et al., 2010; Kuhn et al., 2010). Recent work also reports that ADAM10 loss-of-function mutations are associated with a predisposition to the development of Alzheimer's disease (AD) (Suh et al., 2013), suggesting that interventions leading to reduced ADAM10 activity in the brain may promote the disease, whereas stimulating ADAM10 activity in brain might inhibit development or progression of AD (Lammich et al., 1999; Postina et al., 2004). The ability to modulate ADAM10 activity pharmacologically, however, has been hampered by the lack of structural information about the ADAM10 catalytic domain and its regulation.

ADAMs are single-pass transmembrane proteins with a modular domain organization. ADAM10 and its closest homologue, ADAM17, have an N-terminal

signal sequence and an adjacent prodomain, followed by metalloproteinase, disintegrin, and cysteine-rich domains (Figure 1A). The full-length ADAM precursors are catalytically inactive when the prodomain is intact and associated with the mature enzyme. Previous characterization of both ADAM10 and ADAM17 suggests that the disintegrin and cysteine-rich domains also have an autoregulatory role (Pan and Rubin, 1997), suppressing metalloproteinase activity in the absence of substrates (Stawikowska et al., 2013; Tape et al., 2011). These domains may also direct enzymatic activity by binding proteolytic substrates directly (Janes et al., 2005). Despite the profound importance of ADAM10 in both neurodegenerative disease and Notch signaling, no structural data are currently available for the full-length ectodomain of this protein, leaving unresolved the question of how disintegrin and cysteine-rich domains modulate ADAM activity.

Here, we use X-ray crystallography to determine the structure of the complete ADAM10 ectodomain in isolation and in complex with a non-modulatory antibody at resolutions of 2.8 Å and 3.1 Å, respectively. In both structures, the enzyme adopts a closed conformation in which the cysteine-rich domain precludes access of substrates to the active site. We find that catalytically inactive forms of ADAM10 containing the disintegrin and cysteine-rich domains have dominant-negative inhibitory effects on activity. Conversely, an antibody with an epitope overlapping the autoinhibitory interface enhances the catalytic activity of the enzyme. Together, these studies reveal the molecular basis for regulation of

ADAM10 proteolysis and provide a roadmap for its therapeutic modulation in neurodegenerative diseases and cancer.

RESULTS

Overall structure of ADAM10

In order to elucidate the basis for ADAM10 substrate selectivity and its potential modulation by the disintegrin and cysteine-rich domains, we determined the structure of the mature ADAM10 ectodomain to 2.8 Å resolution by X-ray crystallography (Figure 1 and Table 1). Four copies of the protein are present in the asymmetric unit (Supplementary Figure S1A, related to Figure 1). Remarkably, these are arranged as two pairs of protomers in which the C-terminal tail of one protomer extends into the active site of its partner, mimicking a peptide substrate. The metalloprotease domains of the four protomers are highly similar to one another, with pairwise RMSD values of 0.4 – 0.5 Å (over 741 peptide backbone atoms; Supplementary Figure S1B, related to Figure 1). The interdomain arrangement is preserved in each of the four copies, with only subtle differences observed in the orientation of the disintegrin domain with respect to its flanking metalloproteinase and cysteine-rich domains.

The ADAM10 extracellular domain adopts a compact conformation that resembles an arrowhead, with the metalloproteinase domain enveloped by the

disintegrin and cysteine-rich (D+C) domains (Figure 1A). The structure likely represents an autoinhibited conformation (see below), because the location of the cysteine-rich domain at the mouth of the peptide-binding groove partially occludes the active site, restricting access of substrate to the specificity pocket for the residue that immediately follows the scissile bond (Figure 1A). The D+C domains contain little secondary structure and adopt a cupped shape, rigidified by a disulfide-bond network and a conserved Ca^{2+}-binding loop as in the isolated D+C region of bovine ADAM10 (PDB ID code 5L0Q; (Atapattu et al., 2016)).

Remarkably, the overall architecture of the ADAM10 ectodomain is completely different from that of its non-catalytic homologue ADAM22 (PDB ID 3G5C; (Liu et al., 2009)), the only other ADAM ectodomain of known structure (Figure 1B). While the individual domains are structurally similar, superimposition of the catalytic domains of ADAM10 and ADAM22 shows striking divergence in the organization of the domains relative to one another. The D+C region of ADAM22 engages a completely different surface of the metalloprotease domain from that observed in our structure, wrapping around its base to situate the cysteine-rich domain on the opposite end of the region corresponding to the catalytic groove (Figure 1B). In ADAM22, the two domains can assume this interdomain arrangement because there is a 5-residue linker between them, but there is no analogous linker in ADAM10.

Because the architectural differences between ADAM10 and ADAM22 are so striking, we also determined the structure of a complex between ADAM10 and the F_{ab} portion of a functionally silent antibody called 11G2 (Arduise et al., 2008) to 3.1 Å by X-ray crystallography (Table 1). Importantly, the structure shows that the overall architecture of ADAM10 in complex with 11G2 is indistinguishable from that of isolated ADAM10 (Supplementary Figure S1C, related to Figure 1). The F_{ab} binds to the disintegrin domain 40 Å away from the metalloprotease active site and is equally removed from the cysteine-rich domain, consistent with the observation that it does not modulate ADAM10 activity or function. The specificity of 11G2 for human ADAM10 likely results in part from the recognition of ADAM10 residue R493 by 11G2 heavy chain residues in CDR loops two and three, including W52, which makes van der Waals contacts, and D98, which lies within hydrogen bonding distance (Supplementary Figure S1D, related to Figure 1). In complementary studies, the ADAM10-11G2 F_{ab} complex was visualized by negative stain electron microscopy (EM) and single-particle averaging, producing a 3D reconstruction that is in excellent agreement with our crystallographic studies. The optimal fit of the X-ray structure into the independent EM 3D model (Supplementary Figure S2, related to Figure 1) confirms that the autoinhibited architecture of ADAM10 seen in the X-ray structures is representative of its preferred conformation in solution.

Catalytic Domain and Substrate Recognition

The ADAM10 catalytic domain has key structural features found in active sites of other representative enzymes from the ADAM, matrix metalloprotease, and snake-venom metalloprotease families. The metalloprotease domain core is anchored by a five-stranded β-sheet, the edge of which lines one side of the active site cleft (Figure 2A). Below the cleft is a central helix, which defines the "base" of the active site. As in other adamalysins, this helix includes the HExxH motif that supplies two of the histidines that coordinate the bound zinc ion (H383 and H387) and the glutamate residue (E384) that participates in acid/base catalysis, with the third histidine of the zinc binding motif (H393) situated on the loop following this helix (Figure 2A). C-terminal to the extended zinc-binding motif is a conserved methionine-turn that packs against the zinc-binding site, burying the M417 side chain as a hydrophobic plug beneath the histidine residues that coordinate the zinc ion.

Each enzyme active site in the crystal is occupied by the C-terminal end of a neighboring protein subunit. One of the zinc-coordination sites is filled by the terminal carboxylate oxygen from residue G655' (where the prime nomenclature indicates a residue in the neighboring subunit). The presence of this terminal carboxylate indicates that the C-terminal histidine tag used to facilitate purification was cleaved off during isolation or crystallization of the protein, resulting in fortuitous capture of an enzyme-product complex (Figure 2B,C). Protease substrate selectivity is determined by enzyme pockets, denoted by S, that recognize substrate residues, denoted by P, followed by numbers indicating

the number of substrate residues N-terminal to the cleavage site. The addition of a prime symbol (e.g. S1' and P1') indicates positions C-terminal to the cleavage site. The small S1 pocket, occupied in the structure by G655', is consistent with the preference for alanine at the P1 position in cleavage experiments performed using peptide libraries (Caescu et al., 2009; Tucher et al., 2014). Main chain hydrogen bonds, formed between L654' of the bound peptide and A331 of the edge strand (β4) that lines the active site pocket, position L654' into a poorly defined S2 pocket, which is likely to accommodate a variety of different side chains. In contrast, there is a well-defined hydrophobic S3 pocket bounded by L301, L330, and W332 that surrounds P653' at the P3 position, consistent with the observed preference for proline and other hydrophobic residues at P3 (Caescu et al., 2009; Tucher et al., 2014).

The pocket most important for ADAM10 substrate selectivity is the S1' site, which exhibits a strong preference for large hydrophobic residues (Caescu et al., 2009; Tucher et al., 2014). In the X-ray structure, the S1' cavity is a deep hydrophobic canyon bounded by V376, I379, T380, I416, and T422, readily explaining the preference for bulky hydrophobic residues, including the aromatic residues phenylalanine and tyrosine, at P1'. In contrast, the S1' cavity of ADAM17 is shallower, constrained by Ala439 and Val440 (Figure 2D), and prefers smaller, non-aromatic hydrophobic residues (Caescu et al., 2009; Tucher et al., 2014).

Binding of a modulatory antibody relieves ADAM10 autoinhibition

The structure of ADAM10 suggests that the cysteine-rich domain precludes access of protein substrates to the S1' and S2' pockets, resulting in autoinhibition (Figure 2B,C). Conservation analysis shows that the catalytic cleft and interface between the cysteine-rich domain and the catalytic domain is conserved, suggesting functional importance (Figure 3A,B). To evaluate the autoinhibition model further, we assayed the catalytic activity of the enzyme using a fluorogenic peptide substrate in the presence and absence of the modulatory antibody 8C7. This antibody binds to a site on the cysteine-rich domain, and the x-ray structure (Atapattu et al., 2016) of a complex between the 8C7 F_{ab} and the isolated D+C region of bovine ADAM10, missing the protease domain, has been solved previously (Figure 3C). Superposition of the intact ADAM10 ectodomain onto this structure reveals that the ADAM10 catalytic domain and 8C7 heavy chain would overlap, resulting in a substantial steric clash (Figure 3D). Therefore, 8C7 binding is sterically incompatible with the autoinhibitory interface, and any conformational change in ADAM10 sufficient to relieve the clash would then result in activation of the enzyme through exposure of the active site. Strikingly, binding of 8C7 to ADAM10 does indeed enhance the catalytic activity of the enzyme toward the peptide substrate, in contrast to the non-perturbing control antibody 11G2, which does not affect the activity of the enzyme toward the same substrate (Figure 3E). Binding of the 8C7 antibody thus relieves ADAM10 autoinhibition toward a peptide substrate, as predicted from the structure; this conclusion is also reinforced by a previous report that the rate of association of the 8C7 antibody

with the isolated D+C domain is more rapid in the absence of the metalloprotease domain than in its presence (Atapattu et al., 2012).

Catalytically inactive proteins containing the D+C region show dominant-negative activity

To test whether the D+C region exerts an inhibitory effect on the cleavage of ADAM10 substrates in cells, we first employed a well-established Notch signaling cells co-culture assay using DLL4 as ligand to stimulate the activation of a Notch-responsive reporter gene. When cells expressing a Notch1-Gal4 chimera are stimulated with DLL4-expressing cells, a 15-fold induction of the luciferase reporter gene is observed. When a catalytically inactive variant of ADAM10 bearing the E384A active site mutation is co-transfected into the receptor-expressing cells, there is a dose-dependent attenuation of the reporter signal (Figure 4A,B). To test whether this inhibitory effect is exerted by the isolated D+C region, we examined truncated proteins lacking the ADAM10 catalytic domain (ΔMP), or lacking the entire extracellular region (ΔEC). The attenuation of the Notch response by the ΔMP-ADAM10 protein is comparable to that observed using the E384A protein, whereas the ΔEC protein does not inhibit Notch activation (Figure 4A, B).

To examine whether the inhibitory activity is specific to the D+C region of ADAM10, we compared the ΔMP region of ADAM17, which attenuates ADAM17-

mediated shedding of TNFα (Solomon et al., 1999) to that of ADAM10 in the Notch activation assay (Figure 4C). In contrast to ΔMP-ADAM10, which significantly suppresses Notch activation, ΔMP-ADAM17 does not (Figure 4C). Together, these data show that the ADAM10 D+C region exerts a specific inhibitory effect on ADAM10 proteolysis when present in the Notch expressing cell.

To test the importance of the D+C region in regulating ADAM10 activity towards another substrate, we developed an assay to measure the proteolysis of amyloid precursor protein (APP) and tested the effects of the ADAM10 variants. Upon transfection into U2OS cells, the extracellular portion of APP is released from the cell surface into the culture media (Figure 4D). Treatment of APP expressing cells with the metalloproteinase inhibitor BB94 suppresses APP shedding into the media and leads to accumulation of mature APP in the cells (Figure 4D). When co-transfected with APP, the catalytically inactive E384A and ΔMP forms of ADAM10 reduce APP ectodomain shedding, whereas the co-transfection of ΔEC does not (Figure 4D and Supplementary Figure S3A, related to Figure 4). These results reinforce the importance of the ADAM10 disintegrin and cysteine-rich domains in regulating the processing of diverse substrates.

ADAM10 proteolysis of Notch occurs in *cis*

ADAM family proteins have been shown to function largely in *cis*, cleaving substrate proteins within the plasma membrane of the same cell. However, it has been suggested that ADAM10 acts in *trans* from the ligand-bearing cell to cleave ephrin-A5 on neighboring receptor-bearing cells (Janes et al., 2005). To test whether ADAM10 cleavage of Notch occurs in *cis* or in *trans*, we engineered an *ADAM10*$^{-/-}$ null U2OS cell line with the CRISPR/Cas9 system (Supplementary Figure S3B,C, related to Figure 5) for use in a series of co-culture reporter assays. The absence of ADAM10 dramatically reduces the response of *ADAM10*$^{-/-}$ U2OS cells expressing the Notch1-gal4 chimera to DLL4-expressing sender cells when compared to parental cells expressing Notch1-gal4 (Figure 5A). This signaling defect is fully rescued by restoration of ADAM10 to the Notch-expressing *ADAM10*$^{-/-}$ cells, indicating that ADAM10 is indeed required for Notch activation in U2OS cells (Figure 5A). Next, we tested whether ADAM10 acts in *cis* or in *trans* to execute S2 cleavage of Notch, by expressing different combinations of ligand and receptor in parental and *ADAM10*$^{-/-}$ cells (Figure 5B, C). When Notch and ADAM10 are not present in *cis*, reporter activity is again dramatically reduced. In line with prior studies (Bozkulak and Weinmaster, 2009; van Tetering et al., 2009), these data firmly establish that ADAM10 and Notch must be present in the same cell (*i.e.,* in *cis*) for activation to occur.

DISCUSSION

Here, we report the structure of the ADAM10 ectodomain, providing fundamental insights into how substrate selectivity and regulation of catalytic activity is

achieved in this important representative of the ADAM family of metalloproteases. Full-length ADAM precursors are catalytically inactive when the prodomain is intact, with the latent catalytic activity of the metalloprotease revealed only upon cleavage of the precursor during transport to the cell surface and release of the prodomain from the mature enzyme. The structure presented in this work reveals an unanticipated additional mode of autoregulation intrinsic to the mature enzyme, associated with an intramolecular interface between the disintegrin/cysteine rich-region and the metalloprotease active site. The masking of the active site of the enzyme by the cysteine-rich domain after prodomain release builds in a “fail-safe” mechanism of restricting substrate access that prevents broad-spectrum activity of the mature protease at the cell-surface, providing an additional layer of control beyond the requirement for prodomain release.

Other studies suggest that these two layers of regulation are also shared by the related ADAM family member ADAM17. Like ADAM10, ADAM17 is synthesized as a latent precursor, which requires the removal of a prodomain to be catalytically active. Studies probing the reactivity of a tight-binding inhibitor of ADAM17 indicate that inhibitor access to the active site is rapidly stimulated by a step independent of prodomain removal (Le Gall et al., 2010). In addition, the active-site directed endogenous inhibitor TIMP3 binds with 30-fold faster association kinetics to the isolated ADAM17 catalytic domain than to the complete, mature ectodomain (Tape et al., 2011), pointing again to an analogous

autoregulatory role for the disintegrin and cysteine-rich regions in modulating access of substrates to the ADAM17 active site.

In our studies, we also observe that the disintegrin-cysteine rich region of ADAM10 exhibits dominant inhibitory activity in both Notch signaling and APP shedding assays. These findings further reinforce the notion that this portion of ADAM10 exerts an important modulatory effect on enzyme function. Previous studies have implicated the disintegrin-cysteine rich region of the metalloprotease in enzyme localization and trafficking, and in substrate targeting (*i.e.* as an exosite binding domain). Of note, the cysteine-rich domain of all human ADAMs contains a variable sized loop of 27-55 amino acids with low sequence homology to other ADAM family proteins called the hyper-variable region (HVR), which may be critical for substrate engagement. Alternatively, association of the ADAM10 disintegrin-cysteine rich region with members of the C8 family of tetraspanin proteins has been reported to facilitate ADAM10 export to the cell surface, enhancing its ability to process substrates (Dornier et al., 2012; Jouannet et al., 2016; Noy et al., 2016). Whether the dominant-negative effect arises from competitive *trans* association with fully unmasked metalloprotease active sites, from competition for substrate, or from competition for binding sites on proteins associated with ADAM10 transport, such as the C8-family of tetraspanin proteins, remains to be determined.

The structural and mechanistic studies reported here suggest a model for how ligand-dependent, ADAM10-mediated proteolysis of Notch receptors takes place. The most plausible scenario (Figure 6) is that transient opening of ADAM10 (over a low kinetic barrier and a relatively low value of K_{eq} for [closed]/[open]) is permissive for capture and processing of exposed substrates, such as the mechanically exposed processing site of Notch, or the alpha secretase site of APP. More tantalizing (but perhaps less likely) is the idea that the closed form of ADAM10 is assembled in a complex with Notch, arranged so that application of sufficient mechanical force to expose the Notch processing site simultaneously opens the active site of ADAM10. It is also possible that ADAM10 is localized in a microdomain on the cell surface in complex with other proteins that promote both substrate capture and activation of ADAM10.

The distinct architectural features of the ADAM10 ectodomain also provide a new path forward for the development of selective modulators of ADAM10 function. Others have noted the potential of allosteric activators that stimulate α-secretase cleavage as a therapeutic approach for the treatment of Alzheimer's disease (Lammich et al., 1999; Postina et al., 2004), and compounds that indirectly stimulate α-secretase cleavage without binding to ADAM10 are currently being explored clinically (Wetzel et al., 2017). Conversely, stabilization of the closed conformation with an allosteric antibody or small molecule could provide greatly increased selectivity for inhibition of ADAM10 over ADAM17, analogous to highly selective allosteric inhibitors of enzymes (Chen et al., 2016) and signaling

proteins (Wu et al., 2010). Such inhibitors could find clinical application, for example, in cancers that acquire Herceptin resistance (Feldinger et al., 2014).

AUTHOR CONTRIBUTIONS

Conceptualization, T.C.M.S., B.Z. and S.C.B.; Methodology, T.C.M.S., B.Z., A.C.K., P.A.M., G.S., and S.C.B.; Investigation, T.C.M.S., L.B.K, B.Z., N.S., P.A.M., A.C.K.; Writing T.C.M.S. and S.C.B., with input from D.B.N., G.S., and A.C.K.; Funding Acquisition, T.C.M.S. and S.C.B.; Resources, S.C.B., G.S., D.B.N., E.R., P.W.J., and A.C.K.; Supervision, S.C.B.

ACKNOWLEDGMENTS

This work was supported by a gift from Edward B. Goodnow to S.C.B., NIH awards 5 R01 CA092433 and 1 R35 CA220340 to S.C.B., 5 T32 HL007627 (T.C.M.S.), and NIH award R01 NS038486 to D.B.N. This work is based upon research conducted at the Northeastern Collaborative Access Team beamlines, which are funded by the National Institute of General Medical Sciences from the National Institutes of Health (P41 GM103403). This research used resources of the Advanced Photon Source, a U.S. Department of Energy (DOE) Office of Science User Facility operated for the DOE Office of Science by Argonne National Laboratory under Contract No. DE-AC02-06CH11357.

REFERENCES

Afonine, P.V., Grosse-Kunstleve, R.W., Echols, N., Headd, J.J., Moriarty, N.W., Mustyakimov, M., Terwilliger, T.C., Urzhumtsev, A., Zwart, P.H., and Adams, P.D. (2012). Towards automated crystallographic structure refinement with phenix.refine. Acta Crystallogr D Biol Crystallogr *68*, 352-367.

Andrawes, M.B., Xu, X., Liu, H., Ficarro, S.B., Marto, J.A., Aster, J.C., and Blacklow, S.C. (2013). Intrinsic selectivity of Notch 1 for Delta-like 4 over Delta-like 1. J Biol Chem *288*, 25477-25489.

Arduise, C., Abache, T., Li, L., Billard, M., Chabanon, A., Ludwig, A., Mauduit, P., Boucheix, C., Rubinstein, E., and Le Naour, F. (2008). Tetraspanins regulate ADAM10-mediated cleavage of TNF-alpha and epidermal growth factor. J Immunol *181*, 7002-7013.

Ashkenazy, H., Abadi, S., Martz, E., Chay, O., Mayrose, I., Pupko, T., and Ben-Tal, N. (2016). ConSurf 2016: an improved methodology to estimate and visualize evolutionary conservation in macromolecules. Nucleic Acids Res *44*, W344-350.

Aster, J.C., Pear, W.S., and Blacklow, S.C. (2017). The Varied Roles of Notch in Cancer. Annu Rev Pathol *12*, 245-275.

Aster, J.C., Xu, L., Karnell, F.G., Patriub, V., Pui, J.C., and Pear, W.S. (2000). Essential roles for ankyrin repeat and transactivation domains in induction of T-cell leukemia by notch1. Mol Cell Biol *20*, 7505-7515.

Atapattu, L., Saha, N., Chheang, C., Eissman, M.F., Xu, K., Vail, M.E., Hii, L., Llerena, C., Liu, Z., Horvay, K.*, et al.* (2016). An activated form of ADAM10 is tumor selective and regulates cancer stem-like cells and tumor growth. J Exp Med *213*, 1741-1757.

Atapattu, L., Saha, N., Llerena, C., Vail, M.E., Scott, A.M., Nikolov, D.B., Lackmann, M., and Janes, P.W. (2012). Antibodies binding the ADAM10 substrate recognition domain inhibit Eph function. J Cell Sci *125*, 6084-6093.

Bozkulak, E.C., and Weinmaster, G. (2009). Selective use of ADAM10 and ADAM17 in activation of Notch1 signaling. Mol Cell Biol *29*, 5679-5695.

Bray, S.J. (2016). Notch signalling in context. Nat Rev Mol Cell Biol *17*, 722-735.

Caescu, C.I., Jeschke, G.R., and Turk, B.E. (2009). Active-site determinants of substrate recognition by the metalloproteinases TACE and ADAM10. Biochem J *424*, 79-88.

Chen, V.B., Arendall, W.B., 3rd, Headd, J.J., Keedy, D.A., Immormino, R.M., Kapral, G.J., Murray, L.W., Richardson, J.S., and Richardson, D.C. (2010).

MolProbity: all-atom structure validation for macromolecular crystallography. Acta Crystallogr D Biol Crystallogr *66*, 12-21.

Chen, Y.N., LaMarche, M.J., Chan, H.M., Fekkes, P., Garcia-Fortanet, J., Acker, M.G., Antonakos, B., Chen, C.H., Chen, Z., Cooke, V.G.*, et al.* (2016). Allosteric inhibition of SHP2 phosphatase inhibits cancers driven by receptor tyrosine kinases. Nature *535*, 148-152.

Cho, C., Bunch, D.O., Faure, J.E., Goulding, E.H., Eddy, E.M., Primakoff, P., and Myles, D.G. (1998). Fertilization defects in sperm from mice lacking fertilin beta. Science *281*, 1857-1859.

Cohen, G.H., Silverton, E.W., Padlan, E.A., Dyda, F., Wibbenmeyer, J.A., Willson, R.C., and Davies, D.R. (2005). Water molecules in the antibody-antigen interface of the structure of the Fab HyHEL-5-lysozyme complex at 1.7 A resolution: comparison with results from isothermal titration calorimetry. Acta Crystallogr D Biol Crystallogr *61*, 628-633.

Dornier, E., Coumailleau, F., Ottavi, J.F., Moretti, J., Boucheix, C., Mauduit, P., Schweisguth, F., and Rubinstein, E. (2012). TspanC8 tetraspanins regulate ADAM10/Kuzbanian trafficking and promote Notch activation in flies and mammals. J Cell Biol *199*, 481-496.

Emsley, P., and Cowtan, K. (2004). Coot: model-building tools for molecular graphics. Acta Crystallogr D Biol Crystallogr *60*, 2126-2132.

Escrevente, C., Morais, V.A., Keller, S., Soares, C.M., Altevogt, P., and Costa, J. (2008). Functional role of N-glycosylation from ADAM10 in processing, localization and activity of the enzyme. Biochim Biophys Acta *1780*, 905-913.

Feldinger, K., Generali, D., Kramer-Marek, G., Gijsen, M., Ng, T.B., Wong, J.H., Strina, C., Cappelletti, M., Andreis, D., Li, J.L.*, et al.* (2014). ADAM10 mediates trastuzumab resistance and is correlated with survival in HER2 positive breast cancer. Oncotarget *5*, 6633-6646.

Glomski, K., Monette, S., Manova, K., De Strooper, B., Saftig, P., and Blobel, C.P. (2011). Deletion of Adam10 in endothelial cells leads to defects in organ-specific vascular structures. Blood *118*, 1163-1174.

Hartmann, D., de Strooper, B., Serneels, L., Craessaerts, K., Herreman, A., Annaert, W., Umans, L., Lubke, T., Lena Illert, A., von Figura, K.*, et al.* (2002). The disintegrin/metalloprotease ADAM 10 is essential for Notch signalling but not for alpha-secretase activity in fibroblasts. Hum Mol Genet *11*, 2615-2624.

Janes, P.W., Saha, N., Barton, W.A., Kolev, M.V., Wimmer-Kleikamp, S.H., Nievergall, E., Blobel, C.P., Himanen, J.P., Lackmann, M., and Nikolov, D.B. (2005). Adam meets Eph: an ADAM substrate recognition module acts as a molecular switch for ephrin cleavage in trans. Cell *123*, 291-304.

Jones, J.C., Rustagi, S., and Dempsey, P.J. (2016). ADAM Proteases and Gastrointestinal Function. Annu Rev Physiol *78*, 243-276.

Jorissen, E., Prox, J., Bernreuther, C., Weber, S., Schwanbeck, R., Serneels, L., Snellinx, A., Craessaerts, K., Thathiah, A., Tesseur, I.*, et al.* (2010). The disintegrin/metalloproteinase ADAM10 is essential for the establishment of the brain cortex. J Neurosci *30*, 4833-4844.

Jouannet, S., Saint-Pol, J., Fernandez, L., Nguyen, V., Charrin, S., Boucheix, C., Brou, C., Milhiet, P.E., and Rubinstein, E. (2016). TspanC8 tetraspanins differentially regulate the cleavage of ADAM10 substrates, Notch activation and ADAM10 membrane compartmentalization. Cell Mol Life Sci *73*, 1895-1915.

Kabsch, W. (2010). Xds. Acta Crystallogr D Biol Crystallogr *66*, 125-132.

Kovall, R.A., Gebelein, B., Sprinzak, D., and Kopan, R. (2017). The Canonical Notch Signaling Pathway: Structural and Biochemical Insights into Shape, Sugar, and Force. Dev Cell *41*, 228-241.

Kuhn, P.H., Colombo, A.V., Schusser, B., Dreymueller, D., Wetzel, S., Schepers, U., Herber, J., Ludwig, A., Kremmer, E., Montag, D.*, et al.* (2016). Systematic substrate identification indicates a central role for the metalloprotease ADAM10 in axon targeting and synapse function. Elife *5*.

Kuhn, P.H., Wang, H., Dislich, B., Colombo, A., Zeitschel, U., Ellwart, J.W., Kremmer, E., Rossner, S., and Lichtenthaler, S.F. (2010). ADAM10 is the physiologically relevant, constitutive alpha-secretase of the amyloid precursor protein in primary neurons. EMBO J *29*, 3020-3032.

Lammich, S., Kojro, E., Postina, R., Gilbert, S., Pfeiffer, R., Jasionowski, M., Haass, C., and Fahrenholz, F. (1999). Constitutive and regulated alpha-secretase cleavage of Alzheimer's amyloid precursor protein by a disintegrin metalloprotease. Proc Natl Acad Sci U S A *96*, 3922-3927.

Le Gall, S.M., Maretzky, T., Issuree, P.D., Niu, X.D., Reiss, K., Saftig, P., Khokha, R., Lundell, D., and Blobel, C.P. (2010). ADAM17 is regulated by a rapid and reversible mechanism that controls access to its catalytic site. J Cell Sci *123*, 3913-3922.

Liu, H., Shim, A.H., and He, X. (2009). Structural characterization of the ectodomain of a disintegrin and metalloproteinase-22 (ADAM22), a neural adhesion receptor instead of metalloproteinase: insights on ADAM function. J Biol Chem *284*, 29077-29086.

Liu, P.C., Liu, X., Li, Y., Covington, M., Wynn, R., Huber, R., Hillman, M., Yang, G., Ellis, D., Marando, C.*, et al.* (2006). Identification of ADAM10 as a major source of HER2 ectodomain sheddase activity in HER2 overexpressing breast cancer cells. Cancer Biol Ther *5*, 657-664.

Ludtke, S.J., Baldwin, P.R., and Chiu, W. (1999). EMAN: semiautomated software for high-resolution single-particle reconstructions. J Struct Biol *128*, 82-97.

Maskos, K., Fernandez-Catalan, C., Huber, R., Bourenkov, G.P., Bartunik, H., Ellestad, G.A., Reddy, P., Wolfson, M.F., Rauch, C.T., Castner, B.J.*, et al.* (1998). Crystal structure of the catalytic domain of human tumor necrosis factor-alpha-converting enzyme. Proc Natl Acad Sci U S A *95*, 3408-3412.

McCoy, A.J., Grosse-Kunstleve, R.W., Adams, P.D., Winn, M.D., Storoni, L.C., and Read, R.J. (2007). Phaser crystallographic software. J Appl Crystallogr *40*, 658-674.

Morin, A., Eisenbraun, B., Key, J., Sanschagrin, P.C., Timony, M.A., Ottaviano, M., and Sliz, P. (2013). Collaboration gets the most out of software. Elife *2*, e01456.

Murphy, G. (2008). The ADAMs: signalling scissors in the tumour microenvironment. Nat Rev Cancer *8*, 929-941.

Noy, P.J., Yang, J., Reyat, J.S., Matthews, A.L., Charlton, A.E., Furmston, J., Rogers, D.A., Rainger, G.E., and Tomlinson, M.G. (2016). TspanC8 Tetraspanins and A Disintegrin and Metalloprotease 10 (ADAM10) Interact via Their Extracellular Regions: EVIDENCE FOR DISTINCT BINDING MECHANISMS FOR DIFFERENT TspanC8 PROTEINS. J Biol Chem *291*, 3145-3157.

Overall, C.M., and Blobel, C.P. (2007). In search of partners: linking extracellular proteases to substrates. Nat Rev Mol Cell Biol *8*, 245-257.

Pan, D., and Rubin, G.M. (1997). Kuzbanian controls proteolytic processing of Notch and mediates lateral inhibition during Drosophila and vertebrate neurogenesis. Cell *90*, 271-280.

Penczek, P.A., Grassucci, R.A., and Frank, J. (1994). The ribosome at improved resolution: new techniques for merging and orientation refinement in 3D cryo-electron microscopy of biological particles. Ultramicroscopy *53*, 251-270.

Postina, R., Schroeder, A., Dewachter, I., Bohl, J., Schmitt, U., Kojro, E., Prinzen, C., Endres, K., Hiemke, C., Blessing, M.*, et al.* (2004). A disintegrin-metalloproteinase prevents amyloid plaque formation and hippocampal defects in an Alzheimer disease mouse model. Journal of Clinical Investigation *113*, 1456-1464.

Reiss, K., Maretzky, T., Ludwig, A., Tousseyn, T., de Strooper, B., Hartmann, D., and Saftig, P. (2005). ADAM10 cleavage of N-cadherin and regulation of cell-cell adhesion and beta-catenin nuclear signalling. EMBO J *24*, 742-752.

Sahin, U., Weskamp, G., Kelly, K., Zhou, H.M., Higashiyama, S., Peschon, J., Hartmann, D., Saftig, P., and Blobel, C.P. (2004). Distinct roles for ADAM10 and ADAM17 in ectodomain shedding of six EGFR ligands. J Cell Biol *164*, 769-779.

Scheres, S.H. (2012). RELION: implementation of a Bayesian approach to cryo-EM structure determination. J Struct Biol *180*, 519-530.

Scheres, S.H. (2016). Processing of Structurally Heterogeneous Cryo-EM Data in RELION. Methods Enzymol *579*, 125-157.

Solomon, K.A., Pesti, N., Wu, G., and Newton, R.C. (1999). Cutting edge: a dominant negative form of TNF-alpha converting enzyme inhibits proTNF and TNFRII secretion. J Immunol *163*, 4105-4108.

Stawikowska, R., Cudic, M., Giulianotti, M., Houghten, R.A., Fields, G.B., and Minond, D. (2013). Activity of ADAM17 (a disintegrin and metalloprotease 17) is regulated by its noncatalytic domains and secondary structure of its substrates. J Biol Chem *288*, 22871-22879.

Suh, J., Choi, S.H., Romano, D.M., Gannon, M.A., Lesinski, A.N., Kim, D.Y., and Tanzi, R.E. (2013). ADAM10 missense mutations potentiate beta-amyloid accumulation by impairing prodomain chaperone function. Neuron *80*, 385-401.

Tape, C.J., Willems, S.H., Dombernowsky, S.L., Stanley, P.L., Fogarasi, M., Ouwehand, W., McCafferty, J., and Murphy, G. (2011). Cross-domain inhibition of TACE ectodomain. Proc Natl Acad Sci U S A *108*, 5578-5583.

Tucher, J., Linke, D., Koudelka, T., Cassidy, L., Tredup, C., Wichert, R., Pietrzik, C., Becker-Pauly, C., and Tholey, A. (2014). LC-MS based cleavage site profiling of the proteases ADAM10 and ADAM17 using proteome-derived peptide libraries. J Proteome Res *13*, 2205-2214.

van Tetering, G., van Diest, P., Verlaan, I., van der Wall, E., Kopan, R., and Vooijs, M. (2009). Metalloprotease ADAM10 is required for Notch1 site 2 cleavage. J Biol Chem *284*, 31018-31027.

Weber, S., and Saftig, P. (2012). Ectodomain shedding and ADAMs in development. Development *139*, 3693-3709.

Weskamp, G., Ford, J.W., Sturgill, J., Martin, S., Docherty, A.J., Swendeman, S., Broadway, N., Hartmann, D., Saftig, P., Umland, S*., et al.* (2006). ADAM10 is a principal 'sheddase' of the low-affinity immunoglobulin E receptor CD23. Nat Immunol *7*, 1293-1298.

Wetzel, S., Seipold, L., and Saftig, P. (2017). The metalloproteinase ADAM10: A useful therapeutic target? Biochim Biophys Acta.

Wu, Y., Cain-Hom, C., Choy, L., Hagenbeek, T.J., de Leon, G.P., Chen, Y., Finkle, D., Venook, R., Wu, X., Ridgway, J.*, et al.* (2010). Therapeutic antibody targeting of individual Notch receptors. Nature *464*, 1052-1057.

Yang, Z., Fang, J., Chittuluru, J., Asturias, F.J., and Penczek, P.A. (2012). Iterative stable alignment and clustering of 2D transmission electron microscope images. Structure *20*, 237-247.

FIGURE LEGENDS

Figure 1. ADAM10 Structural Overview. A) Architecture and domain organization. Left panel depicts a schematic of the ADAM10 protein colored by domain. SS: signal sequence; Pro: prodomain; M: metalloproteinase; D: disintegrin; C: cysteine-rich; TM: transmembrane; Cyt; cytoplasmic tail. The red box encompasses the portion of the protein visualized in the X-ray structure. Right panel shows the overall architecture of the mature human ADAM10 ectodomain, colored according to the domain schematic in cartoon representation. The catalytic zinc ion is gray, and a bound calcium ion is shown in orange. Cysteine residues engaged in disulfide bonds are shown as sticks. B) Superposition of ADAM22 (pdb ID code 3G5C) on ADAM10. Proteins are shown in cartoon representation. ADAM10 is colored gray, and ADAM22 domains are colored with the metalloprotease domain magenta, disintegrin domain cyan, cysteine-rich domain green, and EGF-like domain red. ADAM22 calcium ions are colored orange. See also Supplementary Figures S1 and S2.

Figure 2. Structural analysis of the ADAM10 catalytic site. A) Overview of the active site. The metalloproteinase domain is shown in cartoon representation, and the disintegrin and cysteine-rich regions are shown as a gray cartoon with a transparent surface. Key residues at the ADAM10 active site are shown as sticks, and the zinc ion is shown as a gray sphere. Residues 647-655 have been removed for clarity. B) Close-up view, showing C-terminal residues 647-655 of

the adjacent subunit bound in the active site. The metalloproteinase domain is shown in magenta as a transparent molecular surface, with residues contacting the bound product mimic shown as sticks in CPK colors. The C-terminal region of the adjacent subunit is shown as sticks using CPK colors and carbon atoms in yellow. Peptide labels are indicated with a prime mark to distinguish them from labeled active site residues. C) Molecular surface representation. The hydrophobicity of the catalytic domain is shown on a sliding scale from white (polar) to red (hydrophobic). The disintegrin and cysteine-rich regions and the C-terminus of the adjacent subunit are shown as in panels A and B, respectively. The side-chain binding pockets on the enzyme (for S3 – S1') are indicated with dashed lines. D) S1' binding pocket and comparison to ADAM17. The pockets (magenta and beige for ADAM10 and ADAM17, respectively) are viewed as surfaces from "inside" the protein, with the transected protein region shown in gray.

Figure 3. Analysis of ADAM10 Conservation and Autoregulation. A) Conservation analysis shown in an "open book" view. Sequence conservation scores determined using Consurf (Ashkenazy et al., 2016) were mapped onto the surface representation of the ADAM10 ectodomain (middle panel), and onto open book views of the individual D+C (left panel) and metalloprotease (right panel) domains. Conservation scores are colored on a sliding scale from maroon (highest conserved) to teal (least conserved). B) Contact interface analysis. Surface representation of the ADAM10 ectodomain (middle panel) alongside

open book views of the individual D+C (left panel) and metalloproteinase (right panel) domains. Domains are colored as in Figure 1 with residues at the contact interface colored a darker shade. C) Surface representation of the bovine ADAM10 D+C domains (cyan and green, respectively) in complex with the modulatory 8C7 F_{ab} (beige, PDB: 5L0Q). Residues at the contact interface are colored in a darker shade. D) Superposition of the human ADAM10 ectodomain onto the bovine D+C domain complex with the 8C7 F_{ab}. The 8C7 F_{ab} is shown as a transparent surface and the human ADAM10 ectodomain is shown in cartoon representation. The steric clash that would occur between the F_{ab} and the ADAM10 catalytic domain is denoted with a dashed oval. E) Modulation of ADAM10 catalytic activity by the 8C7 F_{ab}. Plots showing hydrolysis of a fluorogenic peptide by purified ADAM10 ectodomain in the presence of increasing concentrations of the 8C7 and 11G2 antibodies are shown. Steady state catalytic rates were plotted as an average of n=3 measurements for each antibody concentration.

Figure 4. Notch1 and APP Processing by ADAM10. A) Schematic representation of the different ADAM10 constructs used in Notch and APP processing assays. B) Notch1-dependent luciferase reporter activity in co-culture assays. U2OS cells transfected with the forms of ADAM10 schematically represented in panel (A) were co-cultured with MS5 cells alone (-DLL4) or with MS5 cells stably expressing human DLL4. C) Notch1-dependent luciferase reporter activity of Notch-expressing U2OS cells co-cultured with DLL4-

expressing cells transefected with either ΔMP-ADAM10 or ΔMP-ADAM17. D) APP shedding assay. Cells transfected with both epitope-tagged APP (FLAG-APP-HA) and the indicated forms of ADAM10 were analyzed by Western blot with anti-FLAG and anti-HA antibodies. APP shed into the media was detected with the anti-FLAG antibody, and APP present in the lysate was detected with anti-HA. The amount of material loaded into each lane was normalized by cell number and assessed by Western blot analysis using an anti-GAPDH antibody. In panels B and C, histograms represent the average of three independent transfections with measurements made in triplicate. Statistical analysis was performed using ANOVA, and a Dunnett's multiple comparison post hoc test was performed comparing test samples to the control. *p <0.05. See Also Supplementary Figure S3.

Figure 5. Notch1 signaling requires ADAM10 in *cis* in U2OS cells. A) Relative Notch1-dependent luciferase reporter activity in U2OS *ADAM10*$^{+/+}$ or U2OS *ADAM10*$^{-/-}$ cells co-cultured with MS5 cells alone (-) or MS5 cells stably expressing DLL4 (+). Addition of ADAM10 (+) to ADAM10$^{-/-}$ U2OS cells restores Notch1-dependent reporter activity when co-cultured with MS5-DLL4 cells. B, C) Co-culture assay adapted for use with U2OS as both the Notch1-expressing and DLL4-expressing cell. Parental or ADAM10 null U2OS cell identity (10$^{+/+}$ or 10$^{-/-}$) for ligand and receptor cells, and DLL4 transfection state of the sending cells are indicated below the bar graph. In panel (C), assays in which ADAM10$^{-/-}$ cells were transfected with ADAM10 are indicated below the graph as +A10.

Histograms represent the average of three independent transfections with measurements made in triplicate. Statistical analysis was performed using ANOVA, and a Dunnett's multiple comparison post hoc test was performed comparing test samples to the control. *p <0.05.

Figure 6. Speculative model for ADAM10-mediated cleavage of Notch receptors. Notch receptors are quiescent in the absence of ligand, with the ADAM10 cleavage site of the receptor masked in a closed conformation ($Notch_{Off}$). ADAM10 likewise favors a closed, autoinhibited (E_{Closed}) conformation over an open one (E_{Open}) that would allow unrestricted access of substrate to the active site. Ligands activate Notch receptors by supplying mechanical force, revealing the ADAM10 processing site (IE**A*V**QS, site of cleavage indicated with an asterisk) in the Notch receptor ($Notch_{On}$), and enabling engagement of $Notch_{On}$ by the active site of the open form of ADAM10 (red arrow). The opening of Notch and ADAM10 dramatically lowers the activation barrier for ADAM10-catalyzed Notch proteolysis ($ES^{\ddagger}$). It is also possible that the D+C region of ADAM10 directly contacts $Notch_{On}$ to stabilize both proteins in their open conformations and promote cleavage (dashed red lines). ADAM10 hydrolysis of Notch releases an S2-processed Notch receptor (P), that is a substrate for further proteloytic processing by γ–secretase.

Table 1. Crystallographic parameters.*

Data Collection	ADAM10	ADAM10-11G2 Fab
Wavelength (λ, Å)	0.979	0.979
Resolution range (Å)	47.19 - 2.80 (2.90 - 2.80)	47.97 - 3.1 (3.211 - 3.1)
Space group	$P2_12_12$	$C222_1$
Unit cell (Å, degrees)	131.42, 188.78, 86.64, 90, 90, 90	79.23, 97.58, 262.72, 90, 90, 90
Total reflections	160809 (15838)	200623 (19415)
Unique reflections	52456 (5184)	18941 (1850)
Multiplicity	3.1 (3.1)	10.6 (10.5)
Completeness (%)	97.37 (97.99)	99.83 (98.76)
Mean I/sigma(I)	4.80 (1.35)	4.05 (0.87)
Wilson B-factor	39.74	57.13
R-sym	0.2598 (0.9681)	0.655 (3.155)
R-meas	0.3137 (1.173)	0.6885 (3.318)
$CC_{1/2}$	0.959 (0.315)	0.959 (0.359)
Reflections used in refinement	52448 (5179)	18916 (1828)
Reflections used for R-free	2655 (262)	1895 (185)
R-work	0.241 (0.341)	0.260 (0.361)
R-free	0.289 (0.396)	0.318 (0.405)
Number of non-hydrogen atoms	13949	6632
Macromolecules	13261	6531
Ligands	332	100
Solvent	356	1
Protein residues	1759	856
RMS (bonds, Å)	0.002	0.002
RMS (angles, degrees)	0.47	0.55
Ramachandran favored (%)	93.74	94.57
Ramachandran allowed (%)	6.02	5.19
Ramachandran outliers (%)	0.06	0.24
Rotamer outliers (%)	1.34	2.28
Clashscore	6.87	8.64
Average B-factor ($Å^2$)	46.73	77.22
Macromolecules	46.87	77.06
Ligands	60.24	88.24
Solvent	28.85	12.97

*Highest shell statistics are reported in parentheses.

STAR METHODS

Contact for Reagent and Resource Sharing

For additional information about reagents and resources, contact the Lead Contact, Stephen Blacklow, at Stephen_Blacklow@hms.harvard.edu.

Experimental Model and Subject Details

Protein expression for crystallography was isolated from conditioned media of *Spodoptera frugiperda* ovarian tissue cells (RRIB: CVCL_0549). SF9 cells were maintained in suspension growing in ESF 921 protein free insect media (Expression Systems) at 27 °C.

Notch and APP shedding assays were pereformed in U2OS cells (RRIB:CVCL_0042). All mammalian cells were maintained at 37 °C in DMEM (VWR Scientific) supplemented with 10% fetal calf serium and penn/strep.

Method Details

Protein Expression and Purification

The extracellular region of ADAM10 including the native signal peptide (residues 1-654) was amplified from a full-length ADAM10 cDNA and subcloned into the baculovirus transfer vector pVL1392 with an additional glycine at position 655 followed by a carboxyl-terminal His_6 tag. Systematic evaluation of the four potential N-linked glycosylation sites revealed that only modification of N278 was essential for proper maturation and secretion of the ectodomain, in agreement with a previous report (Escrevente et al., 2008). We thus introduced N267Q,

N439Q, and N551Q mutations into our pVL1392-ADAM10 construct, generated high-titer baculovirus stocks, and expressed this protein in insect Sf9 cells infected at a density of 4.0 x 10^6 cell/mL. Cells were incubated for an additional 72 h while shaking at 27 °C. The conditioned media was isolated from the cells by centrifugation, supplemented with 20 mM Tris buffer, pH7.5, containing 150 mM NaCl, 5 mM $CaCl_2$, 1 mM $NiCl_2$, and 0.01 mM $ZnCl_2$, re-centrifuged to remove residual debris, and applied to a Ni-NTA column. Bound ADAM10 was washed in 20 mM Tris buffer, pH7.5, containing 150 mM NaCl, 5 mM $CaCl_2$, and eluted in the same buffer supplemented with 500 mM Imidazole. Immediately following elution, the partially purified ADAM10 was concentrated with a centrifugal filter, and isolated on an S200 size exclusion column in in 20 mM sodium cacodylate, pH 6.0, containing 150 mM NaCl, and 5 mM $CaCl_2$. The peak corresponding to monomeric ADAM10 was further purified by ion exchange chromatography on a MonoS column in 20 mM Sodium Cacodylate pH 6.0, using a linear NaCl gradient. The purified protein was buffer-exchanged into 20 mM HEPES buffer, pH7.5, containing 150 mM NaCl prior to flash freezing and permanent storage at -80 °C.

Ascites fluid with ADAM10 11G2 was buffered with 20 mM HEPES, pH 7.5 and captured onto Protein A-sepharose beads. The bound antibody was extensively washed using 20 mM HEPES buffer, pH 7.5, containing 150 mM NaCl and eluted with 100 mM Glycine (pH 3.0). Elution fractions were immediately neutralized with 1 M HEPES buffer, pH 7.5 and the purity of the eluted protein was assessed

on an SDS-PAGE, Coomassie-stained gel. The 11G2 F_{ab} was generated using Ficine-Sepharose (Pierce) according to the manufacturer's instructions. The 11G2 F_{ab} was further purified on an S200 column equilibrated in 20 mM HEPES buffer, pH 7.5, containing 150 mM NaCl. The ADAM10-11G2 F_{ab} protein complex was formed by mixing the two components with ADAM10 in excess, and the complex was isolated from the excess ADAM10 by size exclusion chromatography on an S200 column using 20 mM HEPES buffer, pH 7.5, containing 150 mM NaCl. The protein complex was isolated and concentrated to 10 mg/mL prior to long term storage at -80 °C.

Crystallization, Data Collection, and Structure Determination

Crystals of ADAM10 were grown in 24-well format hanging drops at room temperature. ADAM 10 (2.5 mg/mL) crystals grew after 5 d in 0.26 M ammonium sulfate, 100 mM HEPES pH 7.5, 21.75% PEG8000. Crystals were cryoprotected by supplementing the mother liquor with 10% glycerol (v/v). Individual crystals were flash frozen in liquid nitrogen and stored until data collection.

Data collection was performed at Advanced Photon Source NE-CAT beamline 24 ID-C. Diffraction images were processed and scaled using XDS (Kabsch, 2010). To obtain phases, molecular replacement for all four copies was performed in Phenix with Phaser (McCoy et al., 2007) using chain A from the ADAM17 metalloproteinase structure, PBD ID 1BKC (Maskos et al., 1998) as the search model. A subsequent molecular replacement search was performed, using the

catalytic domain as a fixed partial solution, with a structure of the bovine ADAM10 disintegrin-cysteine rich region fragment, PDB ID 2AO7 (Janes et al., 2005) as the search model. Iterative model building and reciprocal space refinement was performed in COOT (Emsley and Cowtan, 2004) and phenix.refine (Afonine et al., 2012), respectively. Reciprocal space refinement used reciprocal space optimization of xyz coordinates, individual atomic B-factors, NCS restraints, optimization for X-ray/stereochemistry weights, and optimization for X-ray/ADP weights. Model quality was evaluated using composite omit density maps. In final cycles of model building, NCS restraints were removed. Final model quality was assessed using MolProbity (Chen et al., 2010). All crystallographic data processing, refinement, and analysis software was compiled and supported by the SBGrid Consortium (Morin et al., 2013). Data acquisition and refinement statistics are presented in Table 1. Figures were prepared using Pymol (Schrödinger).

Initial crystals of the ADAM10-11G2 F_{ab} complex were grown in 24-well hanging drops at room temperature in 2.0 M ammonium sulfate, 100 mM Tris buffer, pH 8.5, containing 2% PEG400. These crystals were crushed to create a microseed stock, and used to grow additional single crystals at room temperature in 2.23 M ammonium sulfate, 100 mM Tris buffer, pH 8.5, containing 2% PEG400. These crystals were cryoprotected by supplementing with 10% glycerol, flash frozen, and stored in liquid nitrogen until data collection.

Data collection for the ADAM10-F_{ab} complex was performed at Advanced Photon Source NE-CAT beamline 24 ID-C and GM/CA beamline 23 ID-B. The complete data set was obtained by merging diffraction data from two isomorphic crystals in XDS. Initial phases were obtained by molecular replacement using F_{ab} heavy and light chains from PDB ID 1YQV (Cohen et al., 2005) followed by placement of the ADAM10 model generated above. Iterative model building and reciprocal space refinement was performed in COOT and phenix.refine, respectively. Phenix.refine used reciprocal space optimization of xyz coordinates, individual atomic B-factor, optimization for X-ray/stereochemistry weights, and optimization for X-ray/ADP weights. Data acquisition and refinement statistics are presented in Table 1.

Single-particle EM analysis

Samples were prepared for electron microscopy using a conventional negative staining protocol (Peisley and Skiniotis, 2015). The negative stained samples were imaged at room temperature with a Tecnai T12 electron microscope operated at 120 kV using low-dose procedures. Images were recorded at a magnification of ×71,138 and a defocus value of ~1.2 µm on a Gatan US4000 CCD camera. All images were binned (2 × 2 pixels) to obtain a pixel size of 4.16 Å on the specimen level. A total of 19,227 particle projections were excised using Boxer (part of the EMAN 2.1 software suite) (Ludtke et al., 1999) and subjected to two-dimensional reference-free alignment and classification using ISAC (Yang et al., 2012). Representative class averages are shown in

supplemental Figure S2. 3D classification and reconstruction was performed with RELION (Scheres, 2012, 2016). An *ab initio* model generated with VIPER (Penczek et al., 1994) using ISAC 2D averages was used as an initial reference model for maximum-likelihood-based 3D classification of 12,893 particle projections. One stable class accounting for 3,491 particles showed detailed features for both components of the complex and was subjected to 3D refinement. The resulting 3D reconstruction with docked X-ray structure of the ADAM10-11G2 F_{ab} complex is shown in Figure 1C.

Sequence Conservation Analysis

For conservation analysis, we analyzed 356 ADAM10 genes from *bilateria*, using output from the Consurf Seq server. The multiple sequence alignment and the ADAM10 atomic model were then analyzed using the Consurf server, and visualized using default Consurf parameters and colors in Pymol.

Fluorescent ADAM10 Peptide Cleavage Assay

Purified ADAM10, antibody 11G2, and antibody 8C7 were buffer-exchanged into ADAM 10 reaction buffer, which consisted of 25 mM Tris, pH 9.0, containing 2 μM $ZnCl_2$, and 0.005% (w/v) Brij-35. ADAM10 (0.5 μM)-antibody complexes were formed by pre-equilibration for 30 min prior to initiation of the peptide cleavage assay. Peptide cleavage was initiated by mixing 30 μM of a fluorogenic peptide substrate, Mca-PLAQAV-Dpa (R&D Systems Cat# ES003) with ADAM10-antibody complexes at 37 °C, monitoring the progress of reaction by

fluorescence emission (λ_{ex}= 320 nm and λ_{em}= 405 nm) over a time course of 1 h using a SpectraMax M5 Microplate Reader (Molecular Devices).

Cell Lines

All cell lines used in this study (U2OS, MS5, and MS5-DLL4) have been described previously and were maintained in DMEM supplemented with 10% fetal bovine serum and penicillin/streptomycin (Andrawes et al., 2013). To generate an *ADAM10*$^{-/-}$ U2OS cell line, the MIT CRISPR guide design server (crispr.mit.edu) was used to select guide sequences targeting exon 1 of the *ADAM10* gene. DNA guide sequences were purchased (IDT Technologies), annealed in 10 mM Tris, 50 mM NaCl, pH 8, and then subcloned into a pSpCas9 WT-2A-GFP vector using a BsmBI restriction site compatible with overhangs designed into the annealed duplex. The resulting pSpCas9-ADAM10exon1 cDNA was transfected into U2OS cells using Lipofectamine 2000 (Invitrogen). Cells expressing GFP were sorted into 96-well plates by flow cytometry 48–72 h after transfection. Clonal populations were allowed to expand for 2–3 weeks and genomic DNA was extracted from individual clones. For each clone, the targeted *ADAM10* locus was amplified by PCR and TOPO-cloned (Invitrogen) for sequencing. A minimum of 10 clones per cell-line were analyzed to confirm the presence of targeted mutations in ADAM10 exon1. The loss of ADAM10 expression was verified by western blotting with an anti-ADAM10 antibody (Millipore).

Notch Co-culture Assay

To investigate the role of ADAM10 in Delta-like4 (DLL4) stimulated Notch processing, we used a luciferase reporter co-culture assay in which the intracellular ankyrin-repeat domain of Notch is replaced with the Gal4 DNA-binding domain (Andrawes et al., 2013; Aster et al., 2000). On day 1, U2OS cells in 6-well plates were transfected with a reporter mix containing 1.0 µg Gal4-Luciferase, 0.02 µg pRenilla, 0.75 µg Notch1-Gal4, and 0.75 µg of pRK5M-ADAM10 or pcDNA3.1 using Lipofectamine 2000. On the following day, transfected cells were split and mixed with either MS5 control or MS5-DLL4 ligand-expressing cells, and then the mixed cells were co-cultured in 96-well plates. Ater 24 h of co-culture, firefly and *Renilla* luciferase activities were measured in triplicate on a dual-injector luminometer (Turner Systems) using the Dual Luciferase Assay Kit (Promega). The ratio of firefly to *Renilla* activity in the co-culture with MS5 cells alone (negative control) was normalized to a value of 1. Statistical analysis on three independent transfections was performed using ANOVA, and a Dunnett's multiple comparison post hoc test was performed using GraphPad Prism software (version 5.0). *p <0.05.

ADAM10 rescue studies and analysis of dominant-negative activity of ADAM10 mutants were performed with sequences subcloned into the backbone of the parental pRK5M-ADAM10myc tag plasmid (Addgene #31717) using Infusion ligation (Clonetech). The ADAM10 signal sequence was fused to E454 and A655 for the ΔMP and ΔEC constructs, respectively.

Cellular APP Processing Assay

To create a form of APP with an N-terminal FLAG epitope and a C-terminal HA epitope, an C-terminal HA epitope tag was inserted into the FLAG-APP plasmid pCAX FLAG-APP (Addgene #30154) by anchored PCR mutagenesis. To probe APP ectodomain release, U2OS cells in 6-well plates were transfected with 1 µg of pCAX FLAG-APP-HA, ADAM10 (varying amounts), and pcDNA3.1 to maintain a consistent total amount of 2 µg DNA/well. The following day, the transfected cells were washed with PBS, the media was replaced, and in some cases was supplemented with 1 µM BB94 or 1 µM Compound E. After an additional 24 h, the conditioned media was analyzed by SDS-PAGE followed by western blotting with an α-FLAG antibody (M1) to detect APP shedding. The cells were washed extensively and the lysate was similarly analyzed by SDS-PAGE and western blotting using the same α-FLAG antibody and an α-HA antibody (Abacam) to assess the amount of APP remaining in the cell lysate.

Statistical Analysis

Bar graphs display the mean ± SD from three independent transfections. P values were calculated by one-way ANOVA, and a Dunnett's multiple comparison post-hoc test was performed using GraphPad Prism software (version 5.0). *p <0.05.

Data and Software Availibility

The two strucutures reported in this paper are deposited in the RCSB Protein Data Bank (PDB) under the codes: 6BE6 and 6BDZ. The Consurf server is a freely available online tool for academic end users developed and maintained by the Ben-Tal laboratory at Tel Aviv University, Israel. All software used for structure determination (XDS, Phenix, Pymol and Coot) is accessible from the Structural Biology Grid (SBGrid) Consortium at Harvard Medical School.

Key Resources Table

REAGENT or RESOURCE	SOURCE	IDENTIFIER
Antibodies		
anti-ADAM10	EMD Millipore	ab19026 RRIB:AB_2242320
anti-HAtag	Abcam	ab9110 RRIB:AB_307019
anti-GAPDH	Cell Signaling	2118S RRIB:AB_561053
anti-ADAM10 (11G2)	Arduise et al., 2008	
anti-ADAM10 (8C7)	Atapattu et. al., 2016	
Chemicals, Peptides, and Recombinant Proteins		
In-Fusion HD Cloning Plus	Clontech	638911
ESF 921 Insect Cell Culture Medium, Protein-Free	Expression Systems	96001
Lipofectamine 2000	Invitrogen	11668019
100% PEG 400	Hampton Research	HR2603
50%w/v PEG 8000	Hampton Research	HR2535
3.5M Ammonium Sulfate	Hampton Research	HR2541
Mca-PLAQAV-Dpa-RSSSR-NH2	R&D Systems	ES0003
Batimastat (BB94)	Sigma-Aldrich	19440
Compound E	EMD Millipore	565790
Critical Commercial Assays		
Mouse IgG1 Fab and F(ab')2 Preparation Kit	Pierce	44980
TOPO™ TA Cloning™ Kit	ThermoFisher	450030
Dual-Luciferase Reporter Assay System	Promega	E1960
BestBac 1.0 Baculovirus Cotransfection Kit	Expression Systems	91100
Deposited Data		
Human ADAM10 structure coordinates	This paper	PDB ID: 6BE6
Human ADAM10-11G2 Fab structure coordinates	This paper	PDB ID: 6BDZ
Experimental Models: Cell Lines		
Spodoptera frugiperda ovarian tissue (SF9)	Expression Systems	94001S RRIB:CVCL_0549

U2OS	ATCC	HTB-96 RRIB:CVCL_0042
U2OS *ADAM10*$^{-/-}$	This paper	
MS-5	Andrawes et al., 2013	
MS-5 DLL4	Andrawes et al., 2013	
4E11 anti-FLAG M1	ATCC	HB-9259 RRIB:CVCL_J730
Recombinant DNA		
pVL1393	Expression Systems	91030
pVL1393 humanADAM10 3NQ Histag	This paper	
pcDNA3.1 (+) hygro	Invitrogen	V87020
pRK5M-humanADAM10	Addgene	31717
pRK5M-humanADAM10 E384A	This paper	
pRK5M-humanADAM10 ∆MP	This paper	
pRK5M-humanADAM10 ∆EC	This paper	
pCAX FLAG-APP	Addgene	30154
pCAX FLAG-APP-HA	This paper	
pSpCas9(BB)-2A-GFP (PX458)	Addgene	48138
pSpCas9(BB) adam10exon1-2A-GFP	This paper	
pRL *Renilla* Luciferase	Promega	E2231
Gal4-*firefly* Luciferase	Aster et al., 2000	
Notch1-gal4	Andrawes et al., 2013	
pcDNA3-∆ProMP-humanADAM17-HAtag	Addgene	65221
Software and Algorithms		
GraphPad Prism v5.0	N/A	https://www.graphpad.com/scientific-software/prism/
SBGrid Consortium	Morin et al., 2013	http://sbgrid.org/software/
XDS	Kabsch, 2010	http://sbgrid.org/software/
Phaser	McCoy et al., 2007	http://sbgrid.org/software/
Phenix.refine	Afonine et al., 2012	http://sbgrid.org/software/
Coot	Emsley and Cowtan, 2004	http://sbgrid.org/software/
Pymol	Schrödinger Team, 2010	http://sbgrid.org/software/

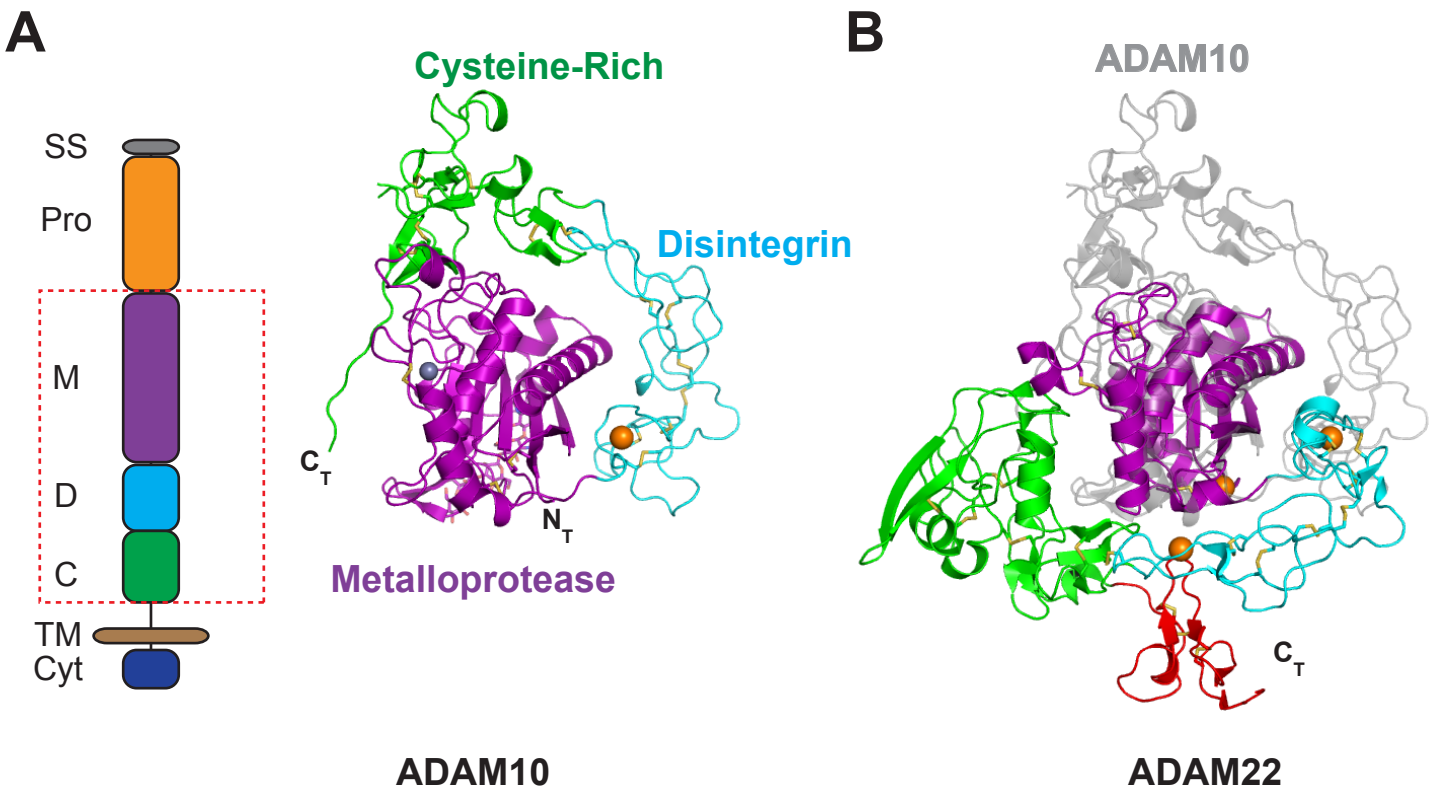
A
SS
Pro
M
D
C
TM
Cyt
Cysteine-Rich
Disintegrin
Metalloprotease
C T
N T
ADAM10
B
ADAM10
C T
ADAM22

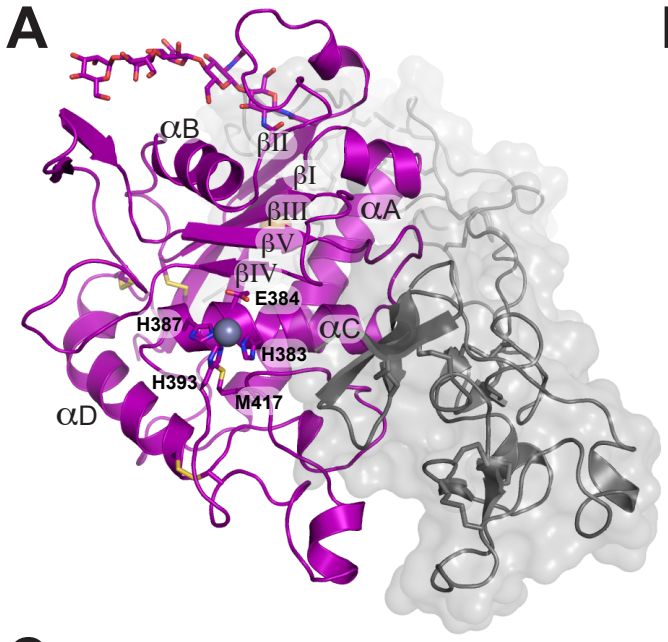
A
αB
βII
βI
βIII
αA
βV
βIV
E384
H387
αC
H383
H393
M417
αD

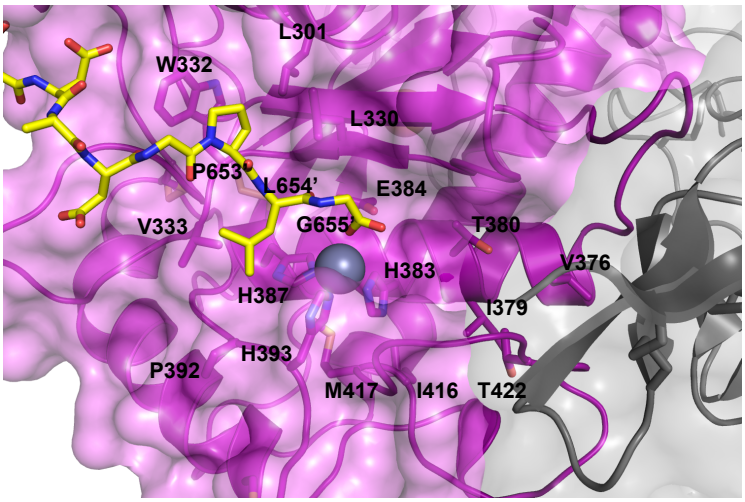
B
L301
W332
L330
P653'
L654'
E384
V333
G655'
T380
V376
H383
H387
I379
H393
P392
M417
I416
T422

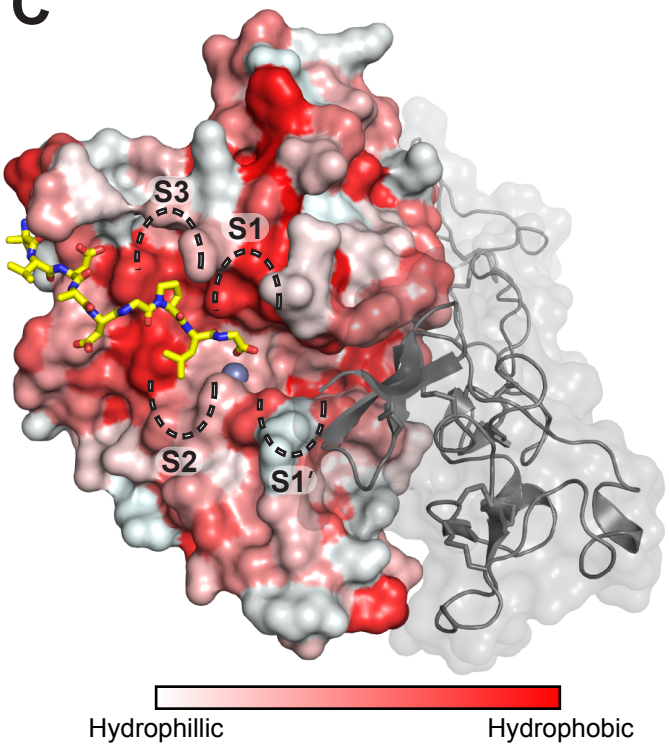
C
S3
S1
S2
S1'
Hydrophillic
Hydrophobic


D
ADAM10 S1'
ADAM17 S1'

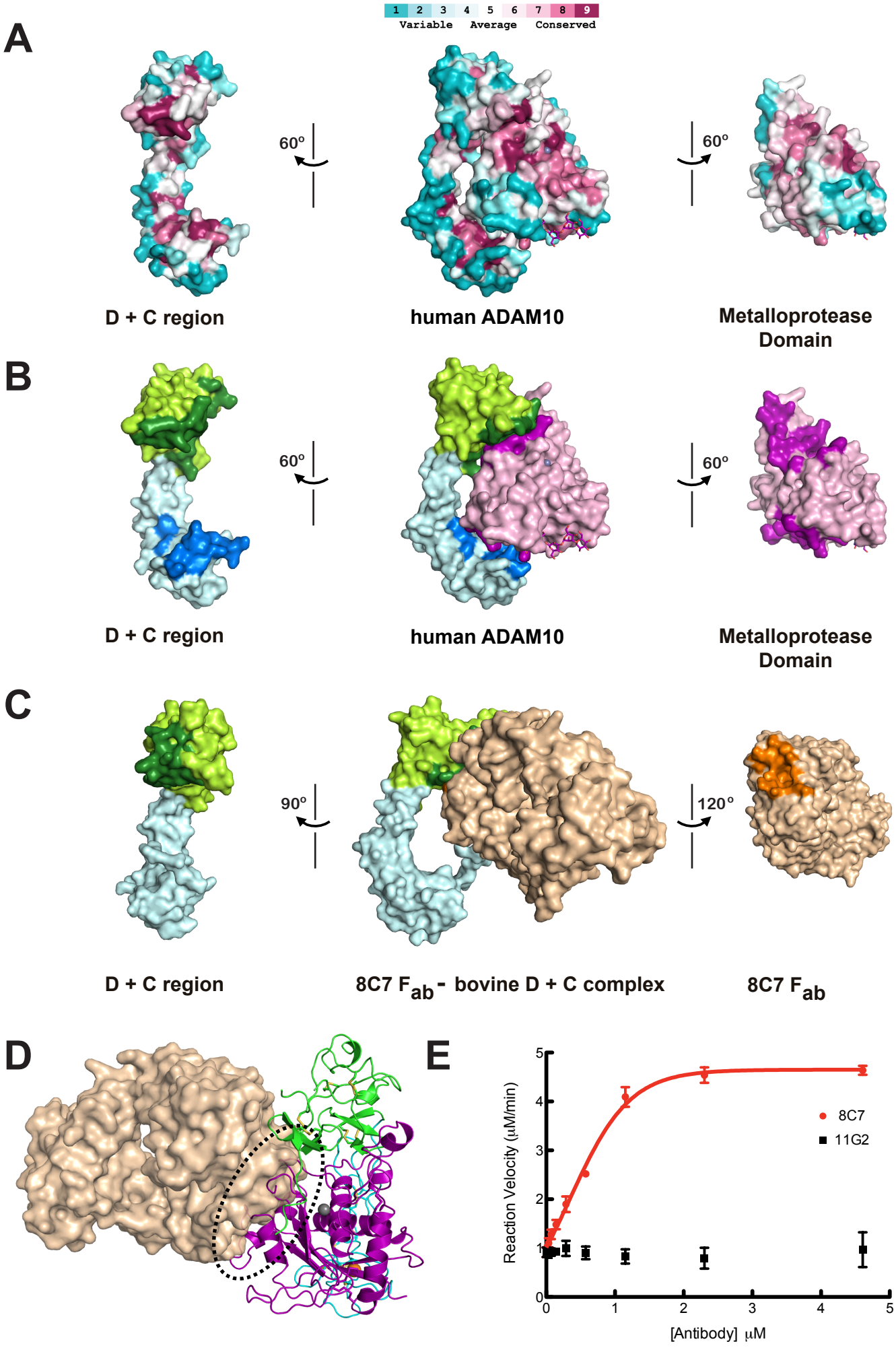
A
1 2 3 4 5 6 7 8 9
Variable Average Conserved
60°
60°
D + C region
human ADAM10
Metalloprotease Domain
B
60°
60°
D + C region
human ADAM10
Metalloprotease Domain
C
90°
120°
D + C region
8C7 Fab - bovine D + C complex
8C7 Fab
D
E
Reaction Velocity (μM/min)
[Antibody] μM
8C7
11G2
0
1
2
3
4
5

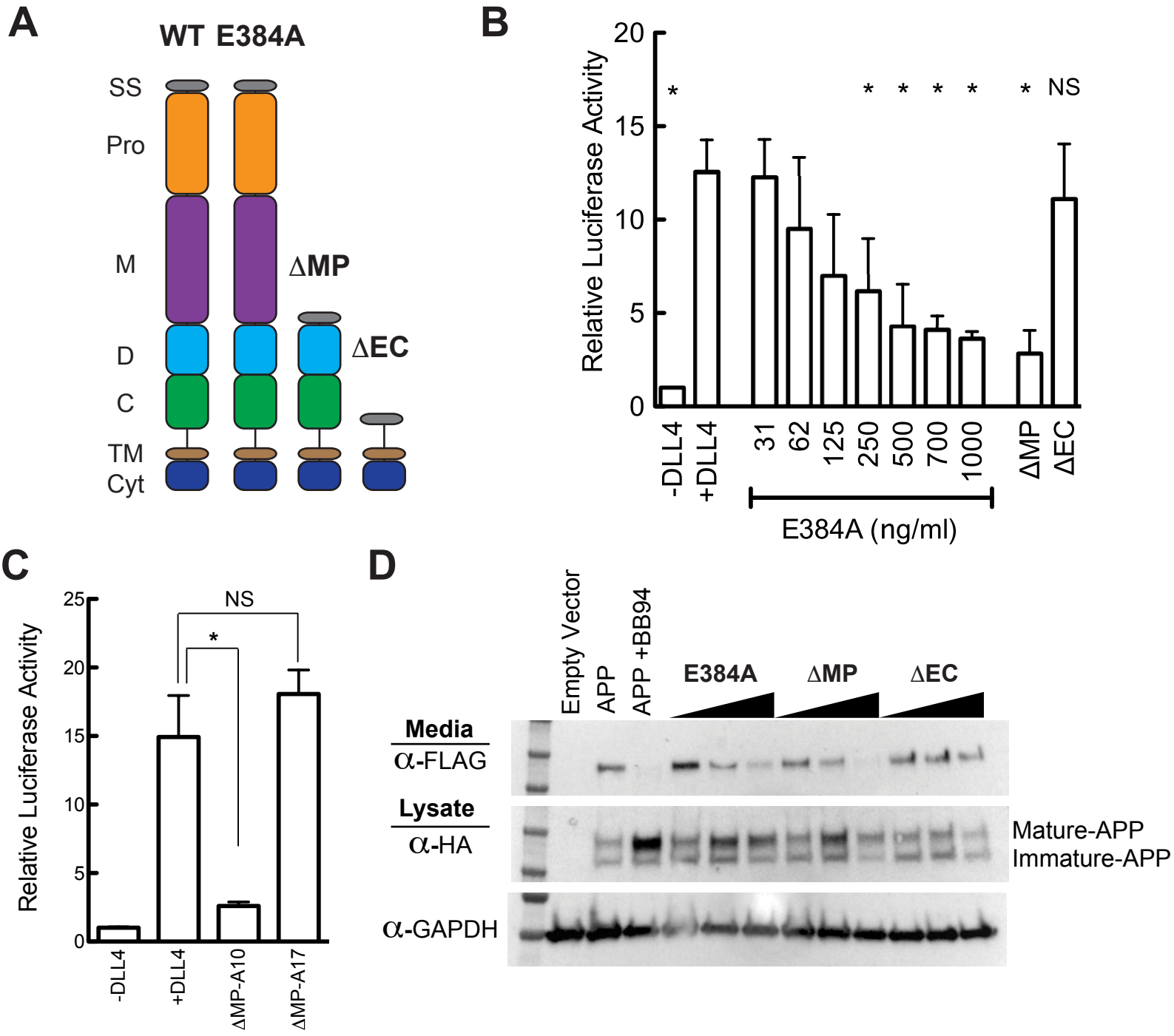
A
WT E384A
SS
Pro
M
D
C
TM
Cyt
ΔMP
ΔEC
B
Relative Luciferase Activity
20
15
10
5
0
*
* * * * * NS
-DLL4
+DLL4
31
62
125
250
500
700
1000
ΔMP
ΔEC
E384A (ng/ml)
C
Relative Luciferase Activity
25
20
15
10
5
0
NS
*
-DLL4
+DLL4
ΔMP-A10
ΔMP-A17
D
Empty Vector
APP
APP +BB94
E384A
ΔMP
ΔEC
Media
α-FLAG
Lysate
α-HA
α-GAPDH
Mature-APP
Immature-APP

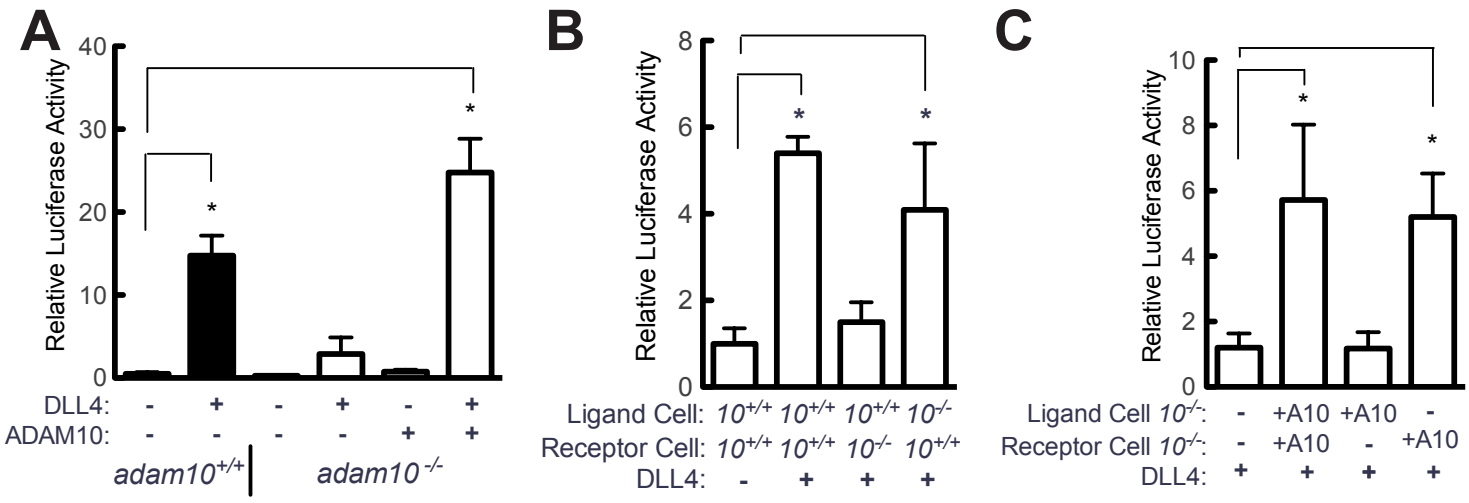
A
Relative Luciferase Activity
40
30
20
10
0
*
*
DLL4: - + - + - +
ADAM10: - - - - + +
adam10+/+
adam10-/-
B
Relative Luciferase Activity
8
6
4
2
0
*
*
Ligand Cell: 10+/+ 10+/+ 10+/+ 10-/-
Receptor Cell: 10+/+ 10+/+ 10-/- 10+/+
DLL4: - + + +
C
Relative Luciferase Activity
10
8
6
4
2
0
*
*
Ligand Cell 10-/-: - +A10 +A10 -
Receptor Cell 10-/-: - +A10 - +A10
DLL4: + + + +

Figure 5